STRESS ELEMENTS FOR ELASTOPLASTICITY: A TREFFTZ FORMULATION WITH PLASTIC CONTROL ON THE BOUNDARY

Flávio Luiz S. Bussamra
ITA - Instituto Tecnológico de Aeronáutica - Divisão de Engenharia Aeronáutica, Brazil
e-mail: flaviobu@aer.ita.br, web-page: http://www.ita.br

Flávio José Silvestre
Undergraduate student; Aeronautical Engineering, Instituto Tecnológico de Aeronáutica, Bolsista PIBIC – CNPq; Brazil
e-mail: flaviosilvestre@hotmail.com

Abstract. The stress model of the hybrid-Trefftz element formulation is applied to the elastoplastic analysis of solids. The stresses are approximated in the domain of the element and the displacements and plastic multipliers are approximated on its boundary. Harmonical and orthogonal hierarchical polynomials are used in stress approximations functions, constrained to solve locally the Beltrami governing differential equation, derived from the associated Papkovitch-Neuber elastic displacement solution. Dirac functions defined at points on the boundary of each element approximate the plastic multipliers. The finite element equations are derived directly from the structural conditions of equilibrium, compatibility, and constitutive relations of the elasticity and plasticity. The non-linear governing system is solved by Newton method. The resulting Hessian matrices are symmetric and highly sparse. All the intervening arrays are defined by boundary integral expressions or by direct collocation. Numerical applications are presented to illustrate the performance of the model.

Keywords. Finite elements; hybrid-Trefftz finite elements; elastoplasticity, three-dimensional plasticity

1. Introduction

The formulation previously proposed in references 1, 2 and 13 for the analysis of three-dimensional elastoplastic problems is based on the independent approximation of three fields: stresses and plastic multipliers are approximated in the element domain and displacements on its static boundary. The stress basis developed in these references for the elastic analysis has shown a good performance in the analysis of tridimensional solids: low sensitivity to geometric irregularities, low sensitivity to mesh distortion, no locking in the incompressibility or near incompressibility regime and good estimates for stresses and displacements. The implicit Euler backward stress integration and the Newton-Raphson method applied to the elastoplastic analysis[3] has shown robustness, reliability and good estimates for collapse loads and displacements[2,13]. But important areas where the plastic criterion was corrupted have been reported.

This paper reports on the application of the hybrid-Trefftz hexahedral stress element to the elastoplastic analysis of solids. The general aspects of the formulation proposed in 1,2 and 13 remain unchanged, but a new set of collocation points used in the plastic control is presented. Plastic multipliers are now approximated on its static boundary.

A polynomial basis for the stresses is derived from Papkovitch-Neuber potentials, that renders an homogeneous solution from Navier equation for stress. This polynomial basis is complete to sixth-degree, with 186 degrees of freedom. The generation of this basis is complete, but presents some spurious modes, which were detected and removed.

The resulting Hessian matrices are symmetric and highly sparse. All intervening matrices and vectors are either defined by boundary integral expressions, which is typical of the Trefftz approach, or computed from direct collocation, as a result of the Dirac approximation of the plastic multiplier field.

Several applications of Trefftz approach display the efficiency on non-linear problems[4,5,6,7,8,9,11,12].

2. Fundamental relations

Let V denote the domain of a typical finite element and Γ is its boundary. Let Γ_u e Γ_σ denote the cinematic and static boundaries ($\Gamma = \Gamma_u \cup \Gamma_\sigma ; \Gamma_u \cap \Gamma_\sigma = \varnothing$). The governing equations are:

$$\mathbf{D\sigma = 0} \quad \text{in V} \tag{1}$$

$$\boldsymbol{\varepsilon} = \mathbf{D}^* \mathbf{u} \quad \text{in V} \tag{2}$$

$$\mathbf{N\sigma = t}_\Gamma \quad \text{in } \Gamma_\sigma \tag{3}$$

$$\mathbf{u = u}_\Gamma \quad \text{in } \Gamma_u \tag{4}$$

In the equilibrium and compatibility conditions (1) to (4), $\mathbf{u}$ is the displacement vector, and vectors $\boldsymbol{\sigma}$ and $\boldsymbol{\varepsilon}$ collect the independent components of stress and strain tensors, respectively. $\mathbf{D}$ is the differential equilibrium operator, and $\mathbf{N}$ is the boundary equilibrium matrix that collects components of the outward normal vector to Γ. $\mathbf{D}$ e $\mathbf{D}^*$ are adjoint differential operators. Body forces and residual stress are not taken on account, for simplicity. $\mathbf{t}_\Gamma$ e $\mathbf{u}_\Gamma$ are vectors that collects the Cauchy tractions (in Γ_σ) and prescribed displacements (in Γ_u), respectively.

The decomposition of the strains into elastic and plastic parts is given by

$$\boldsymbol{\varepsilon} = \boldsymbol{\varepsilon}_e + \boldsymbol{\varepsilon}_p \quad \text{in } V \tag{5}$$

while the elastic relation in terms of the flexibility matrix $\mathbf{f}$ can be written by

$$\boldsymbol{\varepsilon}_e = \mathbf{f}\boldsymbol{\sigma} \quad \text{in } V \tag{6}$$

The plastic flow rule, the normality rule and the Kuhn-Tucker complementarity relations are defined respectively as:

$$\dot{\boldsymbol{\varepsilon}}_p = \dot{\lambda}\,\mathbf{n}(\boldsymbol{\sigma}) \qquad \text{in } V \tag{7}$$

$$\mathbf{n}(\boldsymbol{\sigma}) = \frac{\partial F(\boldsymbol{\sigma})}{\partial \boldsymbol{\sigma}} \qquad \text{in } V \tag{8}$$

$$\dot{\lambda} \geq 0 \ \text{ and } \ F(\boldsymbol{\sigma})\dot{\lambda} = 0 \quad \text{in } V \tag{9}$$

where λ is the plastic multiplier, $\mathbf{n}(\boldsymbol{\sigma})$ collects the outward normal vector to the yield surface and $F(\boldsymbol{\sigma}) \leq 0$ is the yield function.

3. Finite element approximations

3.1. Finite element approximations for elasticity

The formulation presented is based on the direct and independent approximations of stresses components in the domain of the element, increments of plastic multipliers in the domain and on the boundary of the element as well, and the displacements on its static boundary, as shown by expressions (10), (11) and (12) below

$$\boldsymbol{\sigma} = \mathbf{S}\,\mathbf{X} \qquad \text{in } V \tag{10}$$

$$\Delta\lambda = \mathbf{E}_*\,\mathbf{e}_* \quad \text{in } V \text{ and in } \Gamma \tag{11}$$

$$\mathbf{u} = \mathbf{Z}\mathbf{q} \qquad \text{in } \Gamma_\sigma \tag{12}$$

where $\mathbf{S}$, $\mathbf{E}_*$ and $\mathbf{Z}$ are matrices that collect the approximation functions. Vectors $\mathbf{X}$, $\mathbf{e}_*$ e $\mathbf{q}$ are the corresponding weights.

Displacements in the domain of the element can be obtained from the stresses. Equations (2) and (6) lead to

$$\boldsymbol{\sigma} = \mathbf{k}\mathbf{D}^*\mathbf{u} \quad \text{in } V \tag{13}$$

Let $\mathbf{u} = \mathbf{U}\mathbf{X} + \mathbf{u}_r$ be the displacements in the domain of the element, where $\mathbf{u}_r$ collects the rigid-body displacements and $\mathbf{U}$ collects the approximation function related to $\mathbf{S}$, hence

$$\mathbf{S} = \mathbf{k}\mathbf{D}^*\mathbf{U} \quad \text{in } V \tag{14}$$

Trefftz constraint consists on the choice of approximation functions that solve, *a priori*, the Navier equation. Equations (1), (2) and (6) lead to the Navier equation (15), where $\mathbf{k} = \mathbf{f}^{-1}$,

$$\mathbf{D}\mathbf{k}\mathbf{D}^*\mathbf{u} = \mathbf{0} \quad \text{in } V \tag{15}$$

3.2. Stress and displacements approximations in the domain

The associated elastic displacement basis $\mathbf{U}$ associated with the direct stress approximation is derived from the Papkovitch-Neuber solution given by (16) below

$$2G\mathbf{U} = -4(1-\nu)\psi + \nabla(r^t\psi + \phi)\,, \tag{16}$$

where $\boldsymbol{\psi}$ e ϕ are vector and scalar harmonic polynomial displacement potentials, respectively, and $\mathbf{r}$ is the position vector and ∇ the gradient operator. The following potentials were used

$$\varphi_k^L = r^n P_n(\xi_k) \,, \tag{17}$$

$$\phi_k = r_k^n \exp(\theta_k) \quad \text{and} \tag{18}$$

$$\varphi_k = x_k r_k^n \exp(\theta_k) \,, \tag{19}$$

where P_n is the n-th associated Legendre function, $r = \sqrt{x_1^2 + x_2^2 + x_3^2}$, $r_k = \sqrt{x_i^2 + x_j^2}$, $\theta_k = \arctan(x_j/x_i)$, $|\theta_k| \le \pi/4$ and $\xi_k = x_k/r$. φ_k^L potentials and real terms of (18) e (19), when n is an integer, are polynomials, when even permutations of i, j and k are assumed.

The fifteen real functions above, applied to (16), generate 60 polynomial approximation stress functions for each degree n. The Papkovitch-Neuber solution is complete, but linearly dependent modes are generated, and then eliminated by the numerical linear system solver. As it shown in reference 1, the stress approximation basis, defined by equation (14), is self-equilibrated and described by 186 complete, linearly independent polynomial stress modes of sixth degree. Higher degrees are possible, but incomplete basis weree generated. For 7th , 8th and 9th degrees, for example, the stress basis have 237, 294 and 357 independent modes, with deficits of 6, 16 and 31 modes to be completed.

3.3. Displacements approximation in the static boundary

The static boundary displacements are approximated by independent hierarchical polynomial bases, following the Pascal's Triangle scheme in a local coordinate system assigned to each face of the master element.

For a n-th displacement approximation degree, n_z independent displacement modes are generated. n_z is given by

$$n_z = 3\left[1/2(n+1)(n+2)\right]. \tag{23}$$

3.4. Plastic multipliers approximation

The plastic multiplier increment (11) is approximated by Dirac functions $\hat{\delta}(x)$:

$$\mathbf{E_*} = \left[\hat{\delta}(x_1) \,, \hat{\delta}(x_2) \,,\dots,\hat{\delta}(x_N)\right], \tag{24}$$

where the vector $\mathbf{e_*}$ collects the plastic multipliers at points $x_1, x_2, \dots, x_N$. Hence one has

$$\mathbf{e_*} = \left[\Delta\lambda(x_1) \quad \Delta(x_2) \quad \dots \quad \Delta(x_N)\right]^t . \tag{25}$$

Preliminary tests have indicated that Gauss quadrature points provide a good choice for the control of the plastic deformation.

Two sets of Gauss quadrature points are tested here. The first one is defined in the domain of each element2,13. If N is the number of quadrature points chosen for the finite element analysis at each direction, then N^3 points for each element perform the basis for the plastic control.

The second set is defined on the boundary of each element. Each element face has N^2 collocation points, then $6N^2$ points for each element are used in the plastic control.

4. Finite element equations

4.1. Virtual Work equations

With the aid of the virtual work equation

$$\int_V \delta\boldsymbol{\sigma}^t \boldsymbol{\varepsilon} \, dV = \int_{\Gamma_\sigma} (\mathbf{N}\,\delta\boldsymbol{\sigma})^t \mathbf{u} \, d\Gamma + \int_{\Gamma_u} (\mathbf{N}\,\delta\boldsymbol{\sigma})^t \mathbf{u}_\Gamma \, d\Gamma \,, \tag{26}$$

it is possible to derive the following discrete equation

$$\mathbf{F}\,\mathbf{X} - \mathbf{A}\,\mathbf{q} + \int_V \mathbf{S}^t \, \boldsymbol{\varepsilon}_p dV = \mathbf{v} \,, \tag{27}$$

where

$$\mathbf{F} = \int_V \mathbf{S}^t \, \mathbf{f} \, \mathbf{S} \, dV, \tag{28}$$

$$\mathbf{A} = \int_{\Gamma_\sigma} (\mathbf{NS})^t \, \mathbf{Z} \, d\Gamma \quad \text{and} \tag{29}$$

$$\mathbf{v} = \int_{\Gamma_u} (\mathbf{NS})^t \, \mathbf{u}_\Gamma \, d\Gamma. \tag{30}$$

As shown in reference 1, the equivalent boundary integral expression (28) for the symmetric flexibility matrix $\mathbf{F}$ can be obtained by boundary integration, since a self-equilibrated stress approximation basis is used, as follows

$$\mathbf{F} = \int_\Gamma (\mathbf{NS})^t \, \mathbf{u} d\Gamma. \tag{31}$$

On the other hand, the equilibrium condition

$$\int_{\Gamma_\sigma} \delta \mathbf{u}^t \, \mathbf{N\sigma} \, d\Gamma = \int_{\Gamma_\sigma} \delta \mathbf{u}^t \mathbf{t}_\Gamma d\Gamma \tag{32}$$

leads to

$$-\mathbf{A}^t \, \mathbf{X} = -\mathbf{Q}, \tag{33}$$

with

$$\mathbf{Q} = \int_{\Gamma_\sigma} \mathbf{Z}^t \mathbf{t}_\Gamma d\Gamma. \tag{34}$$

4.2. Plastic Strain Time Discretisation

The load is supposed to be applied in N time steps $[t_i, t_{i+1}]$. At instant t_i the displacements, stresses and plastic strains are assumed to be known. At instant t_{i+1} the applied loads or displacements are known. With relations (27), (33) and plastic condition $F(\sigma) \leq 0$ at instant t_{i+1}, the following non-linear system is obtained

$$\begin{cases} \mathbf{F} \, \mathbf{X}_{i+1} - \mathbf{A} \, \mathbf{q}_{i+1} + \int_V \mathbf{S}^t \boldsymbol{\varepsilon}_{p_{i+1}} \, dV = \mathbf{v}_{i+1} & (35a) \\ -\mathbf{A}^t \, \mathbf{X}_{i+1} = -\mathbf{Q}_{i+1} & (35b) \\ F(\boldsymbol{\sigma}_{i+1}) \leq 0 & (35c) \end{cases}$$

The plastic strain increment in time step $[t_i, t_{i+1}]$ is

$$\Delta \boldsymbol{\varepsilon}_p = \int_{t_i}^{t_{i+1}} \dot{\boldsymbol{\varepsilon}}_p \, dt = \int_{t_i}^{t_{i+1}} \dot{\lambda} \, \mathbf{n} \, dt, \tag{36}$$

where $\boldsymbol{\varepsilon}_{p_{i+1}} = \boldsymbol{\varepsilon}_{p_i} + \Delta \boldsymbol{\varepsilon}_p$. The implicit backward Euler integration of the above relation (36) leads to $\boldsymbol{\varepsilon}_{p_{i+1}} = \boldsymbol{\varepsilon}_{p_i} + \Delta \lambda \, \mathbf{n}_{i+1}$. After combining it with (35a), one has

$$\mathbf{F} \, \mathbf{X}_{i+1} - \mathbf{A} \, \mathbf{q}_{i+1} + \int_V \mathbf{S}^t \mathbf{n}_{i+1} \, \Delta\lambda \, dV = \mathbf{v}_{i+1} - \mathbf{e}_{p_i} \quad , \text{ where} \tag{37}$$

$$\mathbf{e}_{p_i} = \int_V \mathbf{S}^t \boldsymbol{\varepsilon}_{p_i} dV. \tag{38}$$

The combination of (11), (37) and (24) leads to

$$\int_V \mathbf{S}^t \mathbf{n}_{i+1} \, \Delta\lambda \, dV = \mathbf{N}_* \mathbf{e}_*, \tag{39}$$

$$\mathbf{N}_* = \int_V \mathbf{S}^t \mathbf{n}_{i+1} \, \mathbf{E}_* \, dV \quad \text{and} \tag{40}$$

$$\mathbf{N}_* = [\mathbf{S}^t(\mathbf{x}_1) \, \mathbf{n}_{i+1}(\boldsymbol{\sigma}(\mathbf{x}_1)) \quad , \quad \mathbf{S}^t(\mathbf{x}_2) \, \mathbf{n}_{i+1}(\boldsymbol{\sigma}(\mathbf{x}_2)) \quad , \quad \dots \quad , \quad \mathbf{S}^t(\mathbf{x}_N) \, \mathbf{n}_{i+1}(\boldsymbol{\sigma}(\mathbf{x}_N))] \tag{41}$$

The weighted form of the yield condition at instant t_{i+1} is given by

$$\int_V \delta\Delta\lambda \; F(\sigma_{i+1}) \, dV = 0, \tag{42}$$

which, with help from (11), leads to

$$\int_V \mathbf{E}_*^t \; F(\sigma_{i+1}) \, dV = 0 \tag{43}$$

The resulting equation system at instant t_{i+1} is presented below

$$\begin{cases} \mathbf{F}\,\mathbf{X}_{i+1} - \mathbf{A}\,\mathbf{q}_{i+1} + \mathbf{N}_* \, \mathbf{e}_* = \mathbf{v}_{i+1} - \mathbf{e}_{p_i} & \text{(44a)} \\ -\mathbf{A}^t \, \mathbf{X}_{i+1} = -\mathbf{Q}_{i+1} & \text{(44b)} \\ \displaystyle\int_V \mathbf{E}_*^t \; F(\sigma_{i+1}) \, dV = 0 & \text{(44c)} \end{cases}$$

4.3. Non-Linear System Solution

Non-linear system (44) can be recast in the following residual form

$$\begin{cases} \mathbf{R}_1(\mathbf{X}_{i+1}, \mathbf{q}_{i+1}, \mathbf{e}_*) = \mathbf{F}\,\mathbf{X}_{i+1} - \mathbf{A}\,\mathbf{q}_{i+1} + \mathbf{N}_* \mathbf{e}_* - \mathbf{v}_{i+1} + \mathbf{e}_{p_i} & \text{(45a)} \\ \mathbf{R}_2(\mathbf{X}_{i+1}, \mathbf{q}_{i+1}) = -\mathbf{A}^t \, \mathbf{X}_{i+1} + \mathbf{Q}_{i+1} & \text{(45b)} \\ \mathbf{R}_3(\mathbf{X}_{i+1}) = \displaystyle\int_V \mathbf{E}_*^t \; F(\sigma_{i+1}) \, dV & \text{(45c)} \end{cases}$$

The system above can be solved by the Newton-Raphson Method. The resulting linear system, which must be solved in each iteration j is:

$$\begin{bmatrix} \mathbf{F} + \mathbf{M}_*^j & -\mathbf{A} & \mathbf{N}_*^{t\,j} \\ & 0 & 0 \\ \text{Symmetric} & & 0 \end{bmatrix} \begin{Bmatrix} \Delta\mathbf{X}^j \\ \Delta\mathbf{q}^j \\ \Delta\mathbf{e}_*^j \end{Bmatrix} = \begin{Bmatrix} \mathbf{R}_1 \\ \mathbf{R}_2 \\ \mathbf{R}_3 \end{Bmatrix}, \quad \text{where} \tag{46}$$

$$\mathbf{M}_* = \int_V \mathbf{S}^t \, \nabla^2 F(\sigma_{i+1}) \, \mathbf{S}\, \mathbf{E}_* \, \mathbf{e}_* \, dV = \sum_{k=1}^N \left[\mathbf{S}^t(\mathbf{x}_k) \, \nabla^2 F(\sigma_{i+1}(\mathbf{x}_k)) \, \mathbf{S}(\mathbf{x}_k) \, \Delta\lambda(\mathbf{x}_k) \right] \tag{47}$$

$$\mathbf{e}_{p_i} = \sum_{k=1}^N \left(\mathbf{S}^t \, \varepsilon_{pi} \right) \tag{48}$$

System (46) is symmetric and highly sparse. Matrices $\mathbf{M}_*$ and $\mathbf{N}_*$ as well as vector $\mathbf{e}_p$ collect information about the so called active collocation points $\mathbf{x}_k$. These are the points for which at the end of each time step one has $F(\sigma_{i+1}(\mathbf{x}_k)) \geq 0$. On the other hand, inactive points, for which $F(\sigma_{i+1}(\mathbf{x}_k)) < 0$, are not represented in the system (47). Which collocation points are active at the end of each time step are not known. The discussion of this issue is left for section 4.5 below.

Stresses, displacements and plastic strains at instant t_{i+1} can be calculated by

$$\sigma_{i+1} = \mathbf{S}\,\mathbf{X}_{i+1} \tag{49}$$

$$\mathbf{u}_{i+1} = \mathbf{Z}\,\mathbf{q}_{i+1} \tag{50}$$

$$\varepsilon_{i+1}^e = \mathbf{f}\,\mathbf{S}\,\mathbf{X}_{i+1} \tag{51}$$

The solution procedure used is the Active Point Method: a set of active points (points with $F(\sigma) \geq 0$) is assumed and the Newton-Raphson method is applied. The inactive points, for which $F(\sigma) < 0$, are not represented in system (46). After each iteration of the Newton-Raphson, all collocation points are evaluated, and a new set of active points is established to perform the next iteration. After the convergence, $F(\sigma) \leq 0$ for every collocation point. This procedure is a variation of the so-called Active Set Method: in this method a set of active points is assumed and the Newton-Raphson method is applied. After the convergence, the set of active points is updated, and the Newton-Raphson method is restarted until the

active set is stabilized. The Active Point Method proved to be much better than the Active Set Method in terms of the overall number of iterations and stability[13].

An alternative method of controlling the load step was implemented. Variable load increments are applied by imposition of an arbitrary increment of internal work[2,12].

5. **Numerical applications**

Two structural elements are used to test the application of the three-dimensional hybrid-Trefftz stress element. The results presented below are directly extracted from the references mentioned or estimated from the graphs presented there when tabulated values are not available. The solutions reported for the hybrid-Trefftz stress element are those directly computed. No smoothing is used in stresses and displacements.

Neither the formulation nor the approximation bases used here constrain the geometry of the finite element, which may be not convex or multiple connected. However, and for simplicity, only one master element is tested in this report, namely the right 8-node hexahedron. The shape functions adopted in the mapping operations typical of isoparametric elements are used here only to support the geometric transformations, as the finite element approximation is implemented on the independent stress and boundary displacement bases described above.

In the tests below, the global scaling is based on three parameters, namely, a length scale L_s, a yield stress scale, Y_s, and a Young modulus scale, E_s, which are identified as the largest values found for these parameters in each application. Thus, the scaled values that replace the actual tractions q, displacements u and plastic multipliers ε_* are the following:

$$\lambda = \frac{q}{Y} \quad ; \quad \delta = \frac{E_s u}{L_s Y} \quad ; \quad \pi = \frac{E_s \varepsilon_*}{Y}$$

For simplicity, in all tests a perfect plastic behavior is assumed, with von Mises yield criterion, with yield stress Y.

Several hybrid-Trefftz stress elements $HTS(d_\sigma, d_{u_\Gamma}, N_p)$ are used in each test, namely, d_σ is the stress approximation degree and d_{u_Γ} is the displacement approximation degree at static boundaries. N_p is the number of collocation points in each direction, say: a) x, y and z, if collocation points on the domain are used; b) ξ_1 and ξ_2 (local axis on each face of hexahedron) if collocation points on the boundaries are used. The total of collocation points in each element is either $(N_p)^3$ or $6(N_p)^2$ for domain and boundaries cases, respectively.

5.1. **Clamped beam tests**

The first set of tests is implemented on the beam fixed at its ends, subject to a uniform transverse load q, shown in Fig.1. The length $L_s = L$, the yield stress $Y_s = Y$ and the Young modulus $E_s = E$ are taken as scaling parameters, and the Poisson ratio used is $\nu = 0.2$.

Five sets of Hybrid-Trefftz stress elements are used, namely HTS(6,3,2), HTS(6,3,4), HTS(6,3,6), HTS(7,3,6) and HTS(8,4,6). These elements have shown best performances in elastoplastic analyses[2,13]. Three, four and five-element meshes are defined in the same figure.

The convergence of the corresponding load-displacement diagrams is presented in Figs. 2, 3 and 4. The displacements δ are the vertical displacements at the centre of the lower face, at midspan. The loads λ are compared with Plastic Hinge Theory limit load $\lambda_r = 0.16$.

As expected, p-refinement is more sensitive in three-element mesh than in the four and five-element meshes. The best HTS solutions are compared in Fig. 5 and in Table 1. Np-refinement induces lower collapse load.
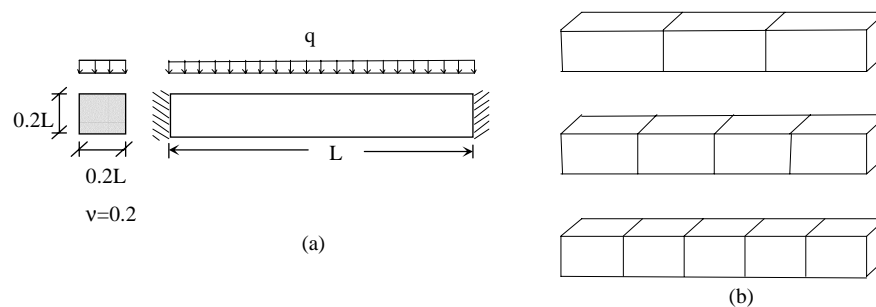

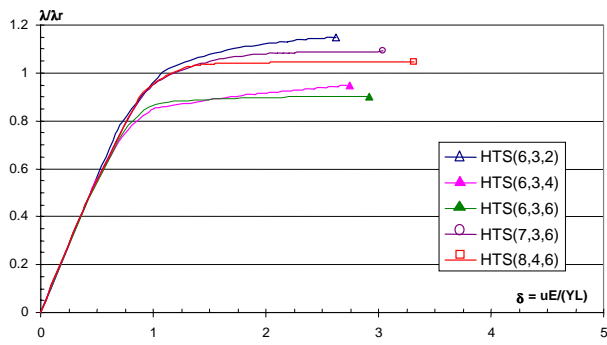Figure1. Elastoplastic analysis of beam: a) geometry b) meshes.

Figure 2. λ-δ diagrams (3-element mesh)
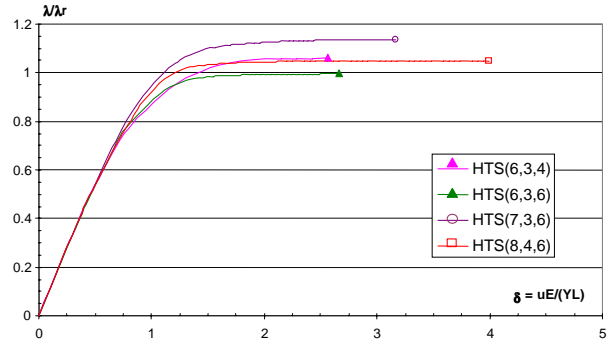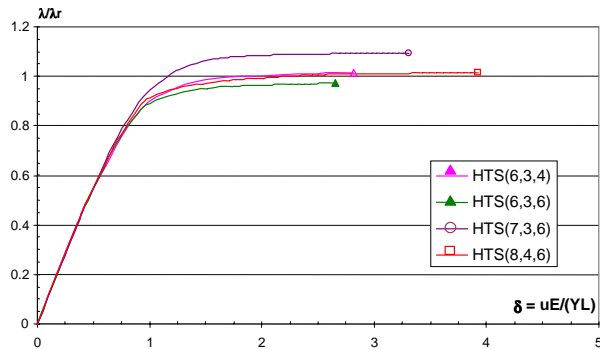

Figure .3. λ-δ diagrams (4-element mesh)
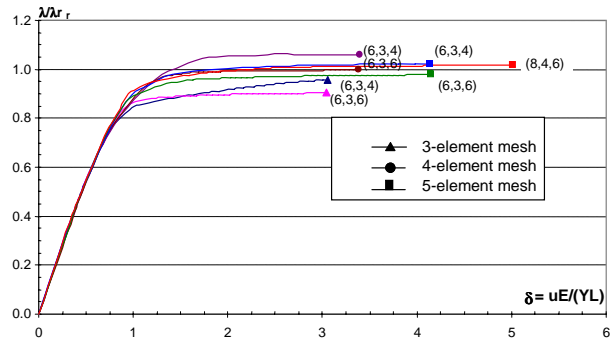

Figure 4. λ-δ diagrams (5-element mesh)

Figure 5. λ-δ diagrams for the beam

lement	Mesh		
	3 elements	4 elements	5 elements
HTS(6,3,4)	0.147	0.169	0.160
HTS(6,3,6)	0.144	0.159	0.154
HTS(8,4,6)	0.167	0.167	0.159

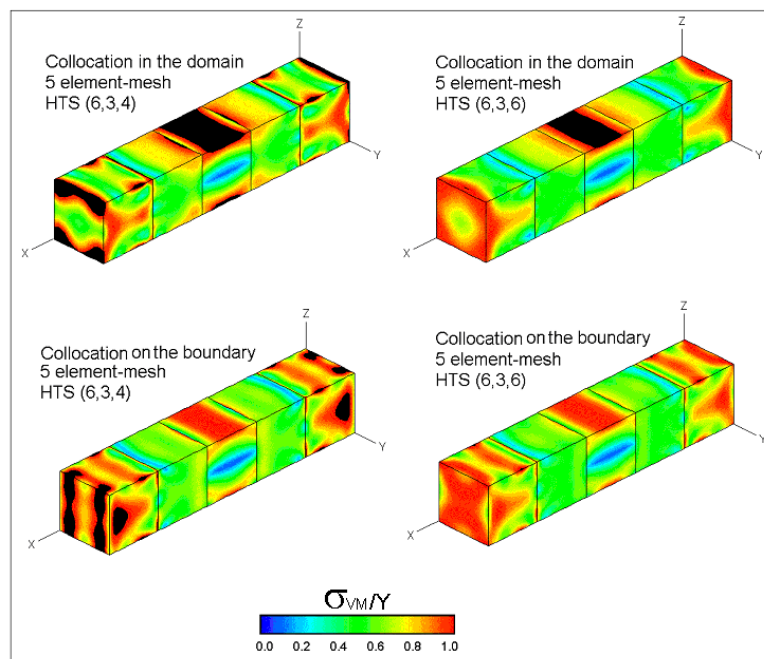Table 1. Collapse load estimates of the beam at $\delta = 2.0$

Figure 6. Von Mises stress distributions in the beam at $\delta = 2.0$

5.2. T-beam tests

A T-short-beam, fixed at z=0, subject to a uniform transverse load q, is shown in Fig.7a. This loading produces bending, shear and torsion in the beam. The length $L_s=L$, the yield stress $Y_s=Y$ and the Young modulus $E_s=E$ are taken as scaling parameters, and the Poisson ratio used is ν=0.2. The 8-element mesh (Fig.7b) is used in Trefftz element tests.
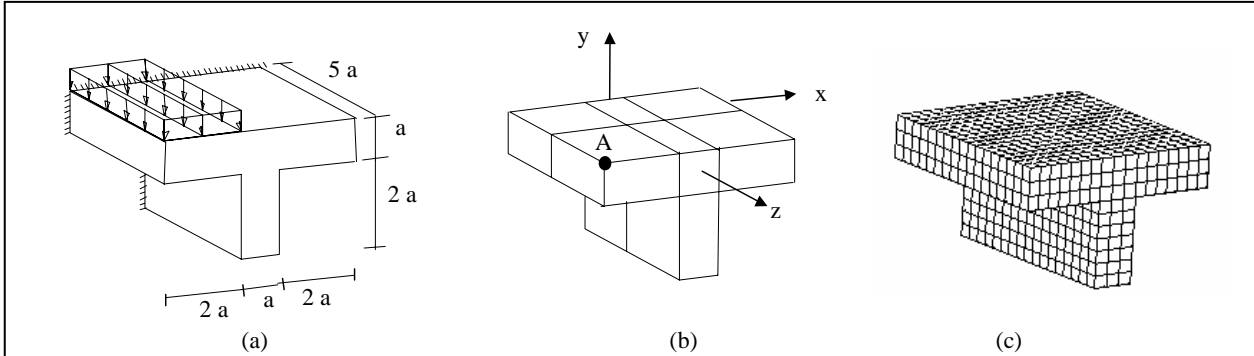

Figure 7. T-Beam. a) geometry and loading; b) 8-element mesh ; c) 1224 element-mesh

The convergence of the corresponding load-displacement diagrams is presented in Fig.8. The displacements δ are the vertical displacements at point A. HTS(7,3,4) Hybrid-Trefftz stress elements are used in both sets of collocation points presented. These results are compared with the 8-node element (HEXA8) of MSC/Nastran[10], with a regular 1224-element mesh (Fig. 7c), and summarized in Table 2. Any volumetric locking was observed. Sparsity found in the Hessian matrix for the HTS(7,3,4) element was 97% at δ=85.
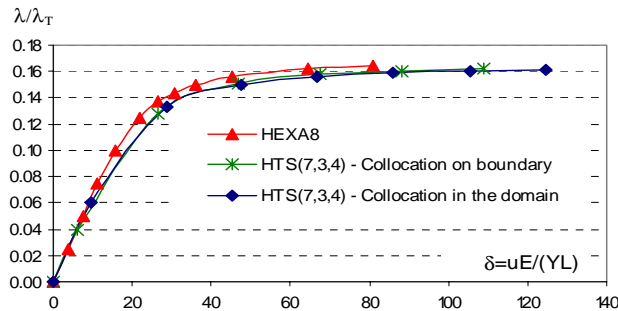

Figure 8. Load-displacement diagrams for the T-beam

Element	Collapse Load	DOF
HEXA8	0,165	5100
HTS(7,3,4) Domain	0,159	3083
HTS(7,3,4) Boundary	0,160	3085

Table 2. Collapse load estimates and Degrees of Freedom at δ = 85

These three tests were executed in a PC (1.50GHz), and the processing times were about 4, 4 and 5 minutes, respectively. The deformed T-beam, at δ=38, with HTS(7,3,4) 8-element mesh, with plastic control on the boundaries, is illustrated in Fig. 10. Gray lines are printed to make displacements easier to be visualized. It can be seen that continuity between boundaries are in general preserved, except in the corner between the loaded surface and the clamped surface.

The deterioration of yield condition is analyzed in Fig. 10, for the 8-element mesh. The legend vanishes from blue ($\sigma_{VM}/Y=0$) to red ($\sigma_{VM}/Y=1$), where σ_{VM} is Von Mises stress. The areas where plastic criterion is corrupted ($\sigma_{VM}/Y>1$) are printed in black. In the domain plastic control, a large corrupted area is printed. At some points the ratio σ_{VM}/Y is greater than 3. For collocation points on the boundary, the corrupted areas are very smaller, and there are no points with the ratio σ_{VM}/Y greater than 1.1.
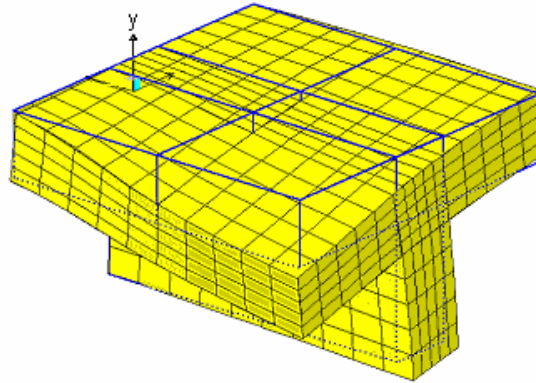
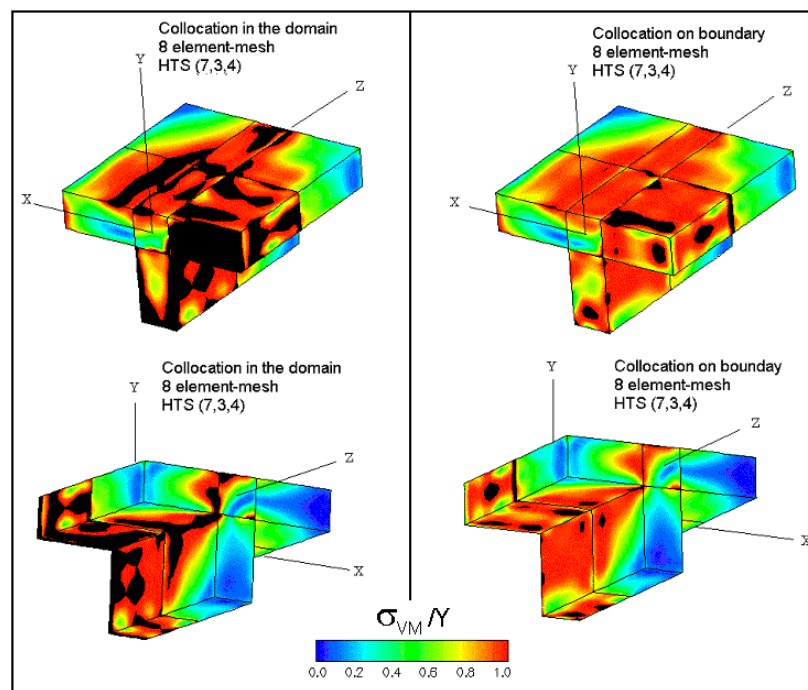Figure 9. Deformed T-beam at δ=38

Figure 10. Von Mises stress distributions in the beam at $\delta = 38$

6. Closure

The results reported above indicated that Gauss quadrature points on element boundary provide a good choice for the control of the plastic deformation for hybrid-Trefftz stress formulation.

The local deterioration of the yield condition presented in [2,3,13] was minimized by controlling the plasticity criterion on boundary collocation points, where the highest Von Mises stresses are known to develop.

The used algorithms have proven to be robust and capable of exploiting the accuracy offered by the hybrid-Trefftz finite element model.

On the other hand, the p-refinement procedure seems to be restricted. To exploit fully the p-hierarchical nature of the formulation it is necessary to enrich the stress approximation bases.

7. Acknowledgement

8. References

1. FREITAS, J.A.T., BUSSAMRA, F.L.S., "Three-Dimensional Hybrid-Trefftz Stress Elements", *International Journal of Numerical Methods in Engineering*, **47**, 927-950, 2000.
2. BUSSAMRA, Flávio Luiz de Silva; PIMENTA, Paulo de Mattos; FREITAS, João António Teixeira de. "Hybrid-Trefftz stress elements for three-dimensional elastoplasticity". Computer Assisted Mechanics and Engineering Sciences, Poland, v. 8, n. 2-3, p. 235-246, 2001.
3. P.M. PIMENTA, P. GOLDENBERG and M.S. MEDRANO, "Applications on mathematical programming for the elastoplastic analysis of solids and structures", in: XV CILAMCE, XV Congresso Ibero Latino-Americano de Métodos Computacionais em Engenharia, São Paulo, Brazil, pp. 1220-1229, (1993).
4. FREITAS,J.A.T., JI,Z.Y. "Hybrid-Trefftz equilibrium model for crack problems", *International Journal for Numerical Methods in Engineering*, **39**, p.569-584,1996.
5. FREITAS, J.A.T., CISMASIU,C., "Formulation of hybrid-Trefftz displacements elements", *Civil Computers*, p.195-202, 1996.
6. PEREIRA,E.M.B.R., "Elementos Finitos de Tensão: Aplicação à Análise Elástica de Estruturas", Tese de Doutorado, Universidade Técnica de Lisboa, 1993.
7. FREITAS,J.A.T., ALMEIDA,J.P.M., PEREIRA,E.M.B.R., "Non-conventional formulations for the finite element method", *International Journal for Numerical Methods in Engineering*, **4**, p.655-678, 1996.
8. FREITAS,J.A.T., "Formulation of elastostatic hybrid-Trefftz stress elements", *Computer Meth. Appl. Mech. Eng.*, **153**, p.127-151, 1997.
9. FREITAS,J.A.T., WANG, Z.M., "Hybrid-Trefftz elements for elastoplasticity", *International Journal for Numerical Methods in Engineering*, 1998.
10. "NASTRAN Theoretical Manual", Washington, DC: NASA, 1972.
11. FREITAS,J.A.T., JI,Z.I., "Hybrid-Trefftz boundary integral formulation for the simulation of singular stress fields", *International Journal for Numerical Methods in Engineering*, **39**, p.281-308, 1996.
12. FREITAS, J.A.T; , WANG, Z.M. "Elastoplastic dynamic analysis with hybrid stress elements", *International Journal of Numerical Methods in Engineering*, **53**, 515-537, 2001.
13. BUSSAMRA, F.L.S., "Hybrid-Trefftz finite elements: an elastoplastic model for three-dimensional solids" (in portuguese), doctor thesis, Escola Politécnica, Universidade de São Paulo, Brazil, 1999.

9. Copyright Notice